Biomedical Research and Therapy 2026, 13(08):8946-8964

Open Access Full Text Article

Original Research

Computational design and characterization of IL-29–GWH1 chimeric protein for targeted cancer therapy

Omeeha Nosha[1], Hafiz Muhammad Rehman[2], Hafiz Muzzammel Rehman[3], Nadeem Ahmed[4], Iram Gull[3], Ayesha Amin[1], Tayyaba Rehman[1], Ariba Asif[1], Hamna Kusar[1], Hamid Bashir[1,*]

[1]*Centre for Applied Molecular Biology (CAMB), 87-West canal, Bank Road, University of the Punjab, Lahore-53700, Pakistan*

[2]*University Institute of Medical Lab Technology, Faculty of Allied Health Sciences, The University of Lahore, Lahore-54590, Pakistan*

[3]*School of Biochemistry and Biotechnology, University of the Punjab, Lahore-53700, Pakistan*

[4]*Centre of excellence in Molecular Biology (CEMB), 87-West Canal, Bank Road, University of the Punjab, Lahore-53700, Pakistan*

Correspondence

Hamid Bashir, Centre for Applied Molecular Biology (CAMB), 87-West canal, Bank Road, University of the Punjab, Lahore-53700, Pakistan

Email: hamid.camb@pu.edu.pk

History

- Received: Jun 16, 2026
- Accepted: Aug 02, 2026
- Published Online: Aug 31, 2026

DOI : 10.15419/bmrat.v13i8.1098

Check for updates

ABSTRACT

Background: A major challenge in modern oncology is developing therapeutics that selectively eliminate tumor cells while sparing healthy tissues. Targeted delivery using engineered chimeric biomolecules can substantially augment therapeutic efficacy and safety. Interleukin-29 (IL-29/IFN-λ1) is a potent type III interferon with antitumor and immunomodulatory properties, whereas GW-H1 is a synthetic cationic antimicrobial peptide that induces caspase-dependent apoptosis in hepatocellular carcinoma (HCC) cells. In this study, an IL-29–GW-H1 chimeric protein was computationally designed by fusing human IL-29 to the GW-H1 peptide via a rigid helical linker [A(EAAAK)$_5$A], followed by recombinant bacterial expression, purification, and in vitro functional validation. **Methods:** Primary amino acid sequences were retrieved and analyzed for physicochemical parameters, secondary structure, and three-dimensional (3D) folding using ProtParam, GOR IV, trRosetta, I-TASSER, and AlphaFold2. Structural stereochemistry was validated using SAVES v6.0 (PROCHECK, ERRAT, Verify3D) and ProSA-web. Molecular docking was performed using ClusPro 2.0 against the IL-28Rα/IL-10Rβ heterodimeric receptor, followed by 100 ns molecular dynamics (MD) simulations in Desmond (Schrödinger) to analyze conformational stability, root mean square deviation (RMSD), root mean square fluctuation (RMSF), dynamic cross-correlation, and binding free energy via MM/GBSA. The chimeric gene was synthesized, cloned into the pET29b(+) expression vector, expressed in *Escherichia coli* BL21(DE3), isolated from inclusion bodies, refolded, and purified via Ni-NTA affinity chromatography. In vitro cytotoxicity was evaluated against HepG2 hepatoma cells and non-tumorigenic HEK293 cells using the MTT assay. **Results:** The refined 3D model exhibited excellent structural quality, with an ERRAT score of 97.06% and 98% of residues situated within the most favored regions of the Ramachandran plot. Molecular docking demonstrated favorable binding of the chimeric construct to the IL-28Rα/IL-10Rβ receptor complex, mediated by 8 salt bridges, 28 hydrogen bonds, and a favorable binding free energy (ΔG = −116.31 kcal/mol). MD simulations over 100 ns confirmed structural equilibration, minimal backbone fluctuations, and a well-defined global free energy minimum. Recombinant IL-29–GW-H1 was successfully expressed in *E. coli* and purified to >98% purity (final yield: 63 mg/L). In MTT cytotoxicity assays, the chimeric protein exhibited significantly higher cytotoxic potency against HepG2 cells (IC_{50} = 16.31 µg/mL) than wild-type IL-29 (IC_{50} = 20.14 µg/mL; $p < 0.001$), while displaying minimal cytotoxicity toward normal HEK293 cells (>60% viability at 25 µg/mL). **Conclusion:** The engineered IL-29–GW-H1 fusion protein demonstrates robust structural stability, strong receptor affinity, and enhanced tumor-selective cytotoxicity against hepatocellular carcinoma cells in vitro. These findings suggest that this novel chimeric construct represents a promising targeted candidate for liver cancer immunotherapy.

Key words: Interleukin-29, GW-H1 peptide, Hepatocellular carcinoma, Fusion protein, Molecular docking, Molecular dynamics simulations, Recombinant expression, Cytotoxicity

INTRODUCTION

Cancer encompasses a heterogeneous group of malignant disorders characterized by recurrent genetic mutations and epigenetic alterations that disrupt essential cellular regulatory pathways[1]. Globally, cancer accounts for approximately ten million deaths annually, representing a major public health burden and a leading cause of mortality in both developed and developing countries[2]. In men, the highest incidence rates are observed in cancers of the prostate, lung and bronchus, colon and rectum, and urinary bladder, whereas in women, breast, lung, colorectal, thyroid, and uterine corpus cancers are among the most frequently diagnosed malignancies[3]. Primary liver cancer is predominantly composed of two histological subtypes: hepatocellular carcinoma (HCC) and cholangiocarcinoma. HCC accounts for the vast majority of primary liver malignancies, represents the third leading cause of cancer-related mortality worldwide, and ranks fifth in cancer incidence among men and seventh

Cite this article : Nosha O, Rehman HM, Rehman HM, Ahmed N, Gull I, Amin A, Rehman T, Asif A, Kusar H, Bashir H. **Computational design and characterization of IL-29–GWH1 chimeric protein for targeted cancer therapy**. *Biomed. Res. Ther.* 2026; 13(08):8946-8964.

among women[4]. Current therapeutic modalities for HCC include surgical resection, liver transplantation, transarterial chemoembolization, and systemic chemotherapy. However, conventional chemotherapeutic agents often lack tumor selectivity and damage healthy tissues alongside malignant cells, resulting in severe dose-limiting toxicities and the rapid emergence of multidrug resistance[5,6]. Consequently, there is an urgent demand for innovative therapeutic strategies that selectively eradicate malignant cells while minimizing off-target adverse effects and therapeutic resistance[7].

Targeted therapy has emerged as a cornerstone of modern oncological intervention due to its selectivity against malignant cells and improved safety profile[8,9]. Engineered chimeric or fusion proteins represent an important class of anticancer biotherapeutics that combine distinct functional domains within a single polypeptide chain[10]. By synergistically integrating distinct structural domains, engineered fusion proteins can acquire novel bioactivities, enhanced pharmacokinetic stability, and superior cell-targeting capabilities[11]. Recombinant constructs that combine an antitumor cytokine with a tumor-targeting or pore-forming peptide offer a promising avenue to augment therapeutic efficacy while sparing non-malignant tissues[12,13]. Previous studies have utilized computational frameworks to design and characterize novel cytokine-peptide fusion constructs, such as IL-15–NGR, demonstrating stable receptor-ligand interactions and enhanced therapeutic selectivity against HCC[9]. Among diverse cytokine families, interleukins exert potent antitumor activity and orchestrate innate and adaptive immune responses against malignancies[14].

In 2003, three closely related cytokines—interleukin-28A (IL-28A), IL-28B, and IL-29—were independently discovered and designated as interferon lambda-2 (IFN-λ2), IFN-λ3, and IFN-λ1, respectively[15]. Collectively classified as type III interferons, they belong to the class II cytokine receptor ligand family[15]. Although IL-29 exists only as a pseudogene in rodents, it is the most abundant and biologically active type III interferon in humans[16]. Both IL-29 and type I IFNs signal predominantly through the Janus kinase/signal transducer and activator of transcription (JAK-STAT) pathway by activating STAT1 and STAT2, with additional minor activation of STAT3 and STAT5[17]. The canonical signaling cascade involves tyrosine phosphorylation of STAT1 and STAT2, which heterodimerize and translocate into the nucleus. Within the nucleus, the heterodimer associates with interferon regulatory factor 9 (IRF9) to form the interferon-stimulated gene factor 3 (ISGF3) transcription factor complex. The assembled ISGF3 complex binds to interferon-stimulated response elements (ISREs) in target promoters, driving the transcription of genes responsible for antiviral, antiproliferative, and pro-apoptotic activities[18].

GW-H1 is an amphipathic cationic antimicrobial peptide of 20 amino acids produced through chemical synthesis[19]. GW-H1 induces caspase-dependent apoptosis in multiple HCC cell lines, including Hep3B, Huh-7, and J5, and suppresses tumor growth in nude mice bearing J5-derived hepatocellular carcinoma xenografts in a dose-dependent manner[20]. Hence, GW-H1 displays potent anticancer properties both in vitro against cultured malignant cells and in vivo in animal tumor models[20].

The present study was designed to computationally construct and experimentally evaluate a novel bifunctional chimeric protein combining human IL-29 with the cytotoxic antimicrobial peptide GW-H1, connected via a rigid alpha-helical linker. We engineered this fusion construct to achieve selective anticancer activity against HCC while minimizing harm to non-cancerous cells. First, the structural, physicochemical, and receptor-binding properties of the chimeric construct were systematically characterized using in silico modeling, molecular docking against the IL-28Rα/IL-10Rβ heterodimeric receptor, and 100 ns molecular dynamics simulations. Subsequently, the chimeric gene was cloned and expressed in *Escherichia coli*, recovered from inclusion bodies, refolded, and purified via immobilized metal affinity chromatography. Finally, in vitro cytotoxicity and selectivity were experimentally validated against HepG2 hepatoma cells and non-tumorigenic HEK293 cells using the MTT assay.

MATERIALS AND METHODS

Construction of IL29-GWH1 fusion protein

The primary amino acid sequence of *Homo sapiens* Interleukin-29 was retrieved in FASTA format from the National Center for Biotechnology Information (NCBI, Accession No. NP_742152). The 20-amino-acid sequence of the GW-H1 peptide was obtained from the study reported by Chen et al.[20]. The three-dimensional crystal structure of the human IL-29 receptor heterodimer, consisting of IL-28Rα and IL-10Rβ (PDB ID: 9BPU), was downloaded from the RCSB Protein Data Bank. To construct the chimeric

molecule, the N-terminal signal peptide (residues 1–19) of IL-29 was excised, and the mature core domain (residues 20–200) was utilized. The GW-H1 peptide was fused to the C-terminus of IL-29 via a rigid alpha-helical linker, $A(EAAAK)_nA$ with $n = 5$ (27 amino acids total). The rigid linker was incorporated between IL-29 and GW-H1 to maintain spatial separation between the two functional domains, prevent unfavorable steric interference, promote independent domain folding, and preserve the biological activities of both components[21,22]. The amino acid sequences utilized in the chimeric construct are listed in Table 1.

Prediction of secondary structure

The secondary structural characteristics of the IL-29–GW-H1 chimeric protein were predicted using the GOR IV web server by submitting the FASTA-formatted amino acid sequence[23]. Conformational properties, including the percentage and distribution of alpha-helices, extended beta-strands, and random coils, as well as solvent accessibility and structural boundaries, were evaluated[24].

Homology modeling, 3D structure prediction, and validation

To predict the tertiary structure of the IL-29–GW-H1 fusion protein, three independent computational modeling platforms were employed: trRosetta, I-TASSER, and AlphaFold2 (ColabFold)[12]. The top-ranked models generated by each server were comparatively evaluated based on their TM-score, C-score, and estimated root mean square deviation (RMSD). The stereochemical quality and structural reliability of the predicted 3D models were assessed using the SAVES v6.0 server, including ERRAT (which determines the overall quality factor), Verify3D (which evaluates the compatibility of the 3D atomic model with its 1D amino acid sequence), and PROCHECK (which generates the Ramachandran plot)[25,26]. Model refinement was subsequently performed using the GalaxyRefine server to optimize side-chain conformations and backbone packing prior to molecular docking.

Physicochemical characterization of IL29-GWH1 chimeric protein

The physicochemical properties of the chimeric construct were calculated using the ExPASy ProtParam tool[27]. Evaluated parameters included the total number and composition of amino acid residues, theoretical isoelectric point (pI), molecular weight, extinction coefficient, in vitro and in vivo estimated half-life, instability index, aliphatic index, and grand average of hydropathicity (GRAVY). In addition, the aqueous solubility profile of the fusion protein was evaluated using the Protein-Sol server.

Prediction of toxicity, allergenicity, and antigenicity

The safety and immunogenic profile of the chimeric protein were evaluated by submitting its amino acid sequence to specialized web servers. Toxicity was predicted using the Neurosnap platform to identify any potentially toxic motifs. Antigenicity was evaluated using the VaxiJen v2.0 server, which assesses protective antigenicity based on physicochemical properties with a default threshold of 0.6[28]. Allergenicity was predicted using AllerTOP v2.0, which examines sequence similarity against known allergenic proteins and epitopes[29].

Soluble expression prediction in Escherichia coli

The solubility and expression propensity of the chimeric construct in *Escherichia coli* were evaluated using the SoluProt server[30]. SoluProt employs a gradient boosting machine learning algorithm trained on 11,436 target proteins from the TargetTrack database to predict soluble protein expression directly from sequence features[31].

Molecular docking and interaction profiling

Protein-protein docking between the IL-29–GW-H1 chimeric construct and the IL-28Rα/IL-10Rβ heterodimeric receptor complex was performed using the ClusPro 2.0 server[32]. ClusPro utilizes a Fast Fourier Transform (FFT) correlation approach (PIPER algorithm) to sample billions of conformations, clusters the lowest-energy docked structures based on RMSD, and performs energy minimization on representative cluster centers. Water molecules and heteroatoms were removed from receptor coordinates prior to docking using the PyMOL Molecular Graphics System. The resulting docked complexes were analyzed for intermolecular interactions—including hydrogen bonds, salt bridges, non-bonded contacts, and buried surface areas—using PDBsum and PDBePISA[33]. The binding free energy of the docked complex was calculated using the MM/GBSA module on the HawkDock server, and the dissociation constant (K_d) was predicted using the PRODIGY server[34].

Table 1: Primary amino acid sequences of the functional domains and rigid helical linker utilized in the construction of the chimeric IL-29–GW-H1 protein.

Protein / Peptide Component	Amino Acid Sequences
Interleukin-29 (IL-29, residues 20–200)	GPVPTSKPTTTGKGCHIGRFKSLSPQELASFKKARDALEESLKLKNWSCSSPVFPGNWDL RLLQVRERPVALEAELALTLKVLEAAAGPALEDVLDQPLHTLHHILSQLQACIQPQPTAGPRP RGRLHHWLHRLQEAPKKESAGCLEASVTFNLFRLLTRDLKYVADGNLCLRTSTHPEST
Rigid Helical Linker [A(EAAAK)$_5$A]	AEAAAKEAAAKEAAAKEAAAKEAAAKA
GW-H1 Peptide (20 aa)	GYNYAKKLANLAKKPANALW

The mature human Interleukin-29 domain (181 residues, corresponding to NCBI NP_742152 minus the N-terminal signal sequence) was fused to the N-terminus of the rigid alpha-helical linker A(EAAAK)$_5$A (27 residues), which in turn was linked to the cationic antimicrobial peptide GW-H1 (20 residues) at the C-terminus, creating a full-length chimeric protein of 228 amino acids.

Molecular dynamics simulations

The docked IL-29–GW-H1–IL-28Rα–IL-10Rβ complex was subjected to all-atom molecular dynamics (MD) simulations using the Desmond simulation package within the Schrödinger software suite[35]. The complex was placed in an orthorhombic simulation box with periodic boundary conditions and solvated using the TIP3P water model. The system was neutralized and physiological ionic strength was established by adding 0.15 M NaCl counterions[36]. The OPLS4 force field was applied. The system was energy-minimized to eliminate steric clashes and equilibrated through standard Desmond multi-step relaxation protocols under NVT and NPT ensembles at a stable temperature of 310 K and a pressure of 1.0 atm. The equilibrated system was then subjected to a 100 ns production MD simulation. Dynamic cross-correlation matrices (DCCM) were computed to analyze correlated and anti-correlated residue motions. Principal component analysis (PCA) was conducted on backbone trajectories, and the first two principal components (PC1 and PC2) were used to construct the 3D Free Energy Landscape (FEL) using the Boltzmann relation[35].

Cloning and recombinant expression of the IL29-GWH1 gene

The codon-optimized IL-29 and IL-29–GW-H1 fusion genes were chemically synthesized by Twist Bioscience (San Francisco, CA, USA) with flanking *Nde*I and *Xho*I restriction sites and cloned into the pET29b(+) expression vector without a native stop codon, thereby incorporating a C-terminal 6×His tag to facilitate affinity purification. Target constructs were verified by restriction endonuclease digestion and PCR amplification with gene-specific primers. Verified plasmids were transformed into chemically competent *E. coli* BL21(DE3) cells via the $CaCl_2$ heat-shock method.

Fermentation and biomass production

For expression of wild-type IL-29 and the recombinant IL-29–GW-H1 fusion protein, shake-flask fermentations were conducted in 2.5 L baffled flasks. Single transformant colonies were inoculated into 50 mL of Luria-Bertani (LB) broth containing 50 μg/mL kanamycin and cultivated at 37 ℃ for 8 h. Pre-cultures were transferred into 500 mL of Terrific Broth (TB) supplemented with kanamycin, incubated at 37 ℃ with shaking at 200 rpm until an optical density at 600 nm (OD_{600}) of 0.6–0.8 was reached, and induced with 1.0 mM isopropyl β-D-1-thiogalactopyranoside (IPTG) for 18 h. Cells were harvested by centrifugation at 6,000 × *g* for 20 min at 4 ℃, and the wet cell biomass was stored at −20 ℃ until processing.

Cell lysis, inclusion body isolation, solubilization, and refolding

Harvested cell biomass was resuspended in lysis buffer (50 mM Tris-HCl pH 8.0, 5 mM EDTA, 1 mM PMSF) and disrupted using a constant cell disruptor (French press system) at 1.5 kbar. Insoluble inclusion bodies (IBs) were separated from soluble host proteins and cell debris by centrifugation at 12,000 × *g* for 30 min at 4 ℃. The isolated IBs were washed

twice with washing buffer (50 mM Tris-HCl pH 8.0, 100 mM NaCl, 1% Triton X-100) and solubilized in solubilization buffer (100 mM Tris-HCl pH 8.0, 6 M guanidine hydrochloride, 2 mM EDTA) with continuous stirring at room temperature for 1 h. Residual insoluble particulates were removed by centrifugation at 8,000 × *g* for 20 min at 4 ℃. The denatured protein solution was refolded by dropwise dilution into refolding buffer (100 mM Tris-HCl pH 8.0, 0.5 M L-arginine, 8 mM EDTA) with gentle stirring at 20 ℃ for 24 h to promote native disulfide formation and proper tertiary folding.

Purification of IL-29 and IL29-GWH1 fusion protein

Refolded protein solutions were desalted, concentrated, and buffer-exchanged by diafiltration using tangential flow filtration cassettes[37]. Purification was carried out by immobilized metal affinity chromatography (IMAC) using a Ni-NTA Sepharose column on an ÄKTA Explorer FPLC system (GE Healthcare). The column was equilibrated with Binding Buffer A (20 mM sodium phosphate, 0.5 M NaCl, pH 7.4). After loading the refolded sample, non-specifically bound host proteins were removed by washing with 10–15 column volumes of Washing Buffer B (20 mM sodium phosphate, 0.5 M NaCl, 20 mM imidazole, pH 7.4). The target His-tagged proteins were eluted using Elution Buffer (20 mM sodium phosphate, 0.5 M NaCl, 0.5 M imidazole, pH 7.4). Eluted fractions were pooled, dialyzed against phosphate-buffered saline (PBS, pH 7.4), and stored at −80 ℃.

Characterization by SDS-PAGE and Western blotting

The purity and molecular weight of purified IL-29 and IL-29–GW-H1 were assessed on 12% SDS-PAGE gels resolved at a constant voltage of 110 V for 150 min using a Hoefer SE260 vertical electrophoresis system. Gels were stained with Coomassie Brilliant Blue R-250 and destained to visualize protein bands. For Western blot confirmation, resolved proteins were electroblotted onto nitrocellulose membranes using a Hoefer Semiphor semi-dry transfer unit. Membranes were blocked with 5% (w/v) non-fat dry milk in Tris-buffered saline with 0.1% Tween-20 (TBST) for 1 h at room temperature, incubated with mouse anti-6×His primary antibody (1:1,000 dilution) for 1 h, washed thoroughly with TBST, and probed with horseradish peroxidase (HRP)-conjugated goat anti-mouse IgG secondary antibody (1:5,000 dilution). Immunoreactive bands were visualized using NBT/BCIP substrate solution.

In vitro cytotoxicity assessment by MTT assay

Human hepatocellular carcinoma HepG2 cells (ATCC HB-8065) and non-tumorigenic human embryonic kidney HEK293 cells (ATCC CRL-1573) were cultured in Dulbecco's Modified Eagle's Medium (DMEM) supplemented with 10% fetal bovine serum (FBS), 100 U/mL penicillin, and 100 µg/mL streptomycin in a humidified incubator with 5% CO_2 at 37 ℃. Cytotoxicity was determined using the 3-(4,5-dimethylthiazol-2-yl)-2,5-diphenyltetrazolium bromide (MTT) assay. Cells were seeded into 96-well culture plates (1×10^4 cells/well) and allowed to adhere overnight. Cells were then treated in triplicate with varying concentrations (5, 10, 15, 20, and 25 µg/mL) of purified wild-type IL-29 or chimeric IL-29–GW-H1 for 24 h. Untreated cells served as negative controls. Following incubation, 10 µL of MTT reagent (5 mg/mL in PBS) was added to each well and incubated for an additional 4 h at 37 ℃. The culture medium was removed, and 100 µL of dimethyl sulfoxide (DMSO) was added to each well to solubilize the purple formazan crystals. Absorbance was measured at 570 nm with a reference wavelength of 630 nm using a microplate spectrophotometer. Percentage cell viability was calculated using the following equation:

$$\text{Cell Viability (\%)} = [(A_{570}A_{630})_{\text{treated}} / (A_{570}A_{630})_{\text{control}}] \times 100$$

Statistical analysis

All quantitative experimental assays were conducted independently in triplicate ($n = 3$), and data are presented as the mean ± standard deviation (SD). Statistical analyses were performed using GraphPad Prism version 7.0 (GraphPad Software, Inc., San Diego, CA, USA). Differences between treatment groups across various concentrations were evaluated using one-way Analysis of Variance (ANOVA) followed by Tukey's post-hoc honestly significant difference (HSD) test. Differences were considered statistically significant at $p < 0.05$ ($^{*}p < 0.05$, $^{**}p < 0.01$, $^{***}p < 0.001$, $^{****}p < 0.0001$).

RESULTS

Construction and sequence architecture of IL29-GWH1 chimeric protein

To generate the chimeric antitumor protein, the primary sequence of mature human IL-29 was linked at

its C-terminus to the synthetic cationic peptide GW-H1 via a rigid alpha-helical linker [A(EAAAK)$_5$A]. The resulting chimeric IL-29–GW-H1 construct consists of a single continuous polypeptide chain of 228 amino acids (Figure 1). The incorporation of the rigid helical linker ensures conformational separation between the cytokine and peptide domains, preventing steric hindrance and improper domain entanglement.

Secondary structure prediction

The secondary structure of the chimeric IL-29–GW-H1 protein was predicted using the GOR IV web server (Figure 2). The analysis revealed that the 228-residue polypeptide chain comprises 140 amino acids in alpha-helical conformations (61.40%), 7 residues in extended beta-strands (3.07%), and 81 residues in random coils (35.53%). The high alpha-helical content is consistent with the structural architecture of type III interferons and helical linkers, imparting enhanced thermodynamic and conformational stability to the chimeric protein [38].

Tertiary structure prediction, validation, and refinement

Homology and ab initio modeling were performed using trRosetta, I-TASSER, and AlphaFold2 to predict the 3D tertiary structure of the IL-29–GW-H1 fusion protein. Comparative assessment of the top models indicated that trRosetta generated the most accurate structure, with a TM-score of 0.829 (Table 2). Stereochemical validation on the SAVES v6.0 server confirmed that the trRosetta model exhibited an initial ERRAT quality factor of 95.15% and placed 96% of residues in the most favored regions of the Ramachandran plot. Following structural refinement using GalaxyRefine, the optimized model displayed further improvements: 98.0% of residues fell within the most favored Ramachandran regions (Figure 3B), with no residues in disallowed regions, and the ERRAT overall quality score rose to 97.06%. ProSA-web analysis yielded an overall model Z-score of –8.09 (Figure 3C), which resides within the distribution typical of experimentally determined native protein structures of comparable size. The ProSA-web energy profile demonstrated consistently negative knowledge-based energy values across the sequence (Figure 3D), confirming overall structural stability.

Physicochemical characterization

The physicochemical properties of the chimeric IL-29–GW-H1 construct were computed using ExPASy ProtParam (Table 3). The 228-residue protein has a molecular weight of 24,729.45 Da and a total atomic count of 3,518. Because positively charged basic residues (Arg + Lys = 32) exceed negatively charged acidic residues (Asp + Glu = 23), the chimeric protein is basic, with a theoretical isoelectric point (pI) of 9.38. The instability index was calculated at 45.32, and the aliphatic index was 86.71, indicating high thermostability. The grand average of hydropathicity (GRAVY) was –0.365, confirming the hydrophilic nature of the construct and its favorable solubility in aqueous environments. The predicted half-life was estimated at 30 h in mammalian reticulocytes in vitro, >20 h in yeast in vivo, and >10 h in *E. coli* in vivo. The molar extinction coefficient was 26,720 M^{-1} cm^{-1} at 280 nm. Protein-Sol solubility analysis yielded a score of 0.677 (Figure 3E), well above the population average threshold of 0.45, confirming high predicted aqueous solubility.

Assessment of toxicity, allergenicity, and antigenicity

Safety profiling conducted via Neurosnap and AllerTOP v2.0 predicted that the chimeric IL-29–GW-H1 protein is non-toxic (overall toxicity score: 0.295) and non-allergenic. Antigenicity evaluation via VaxiJen v2.0 yielded an antigenicity score of 0.50 at a 0.60 threshold, classifying the construct as non-antigenic and suggesting low risk of eliciting adverse neutralizing immunogenicity upon administration.

Soluble expression prediction in Escherichia coli

The SoluProt machine learning algorithm predicted a solubility score of 0.955 for the chimeric IL-29–GW-H1 protein in *E. coli*. Because values exceeding 0.50 indicate high soluble expression probability, this result predicted favorable expression efficiency in recombinant bacterial hosts.

Molecular docking analysis

Molecular docking between the chimeric IL-29–GW-H1 protein and the IL-28Rα/IL-10Rβ heterodimeric receptor was performed using ClusPro 2.0 (Figure 4). The top ten docking clusters generated by ClusPro 2.0 are summarized in Table 4. Cluster 0 contained the largest number of members (39 cluster members) and displayed the lowest energy score of –839.8 kcal/mol and a weighted score of –797.7, representing the most stable and thermodynamically favorable binding mode. Clusters 1 and 2 also exhibited favorable binding scores (–744.0 and –756.4,

Figure 1: Schematic diagram and primary sequence architecture of the engineered chimeric IL-29–GW-H1 fusion protein. Schematic illustration of the recombinant construct design. The 228-amino-acid chimeric protein consists of the mature human Interleukin-29 sequence (residues 20–200, blue, 181 aa) at the N-terminus, linked via a 27-amino-acid rigid alpha-helical linker [AEAAAKEAAAKEAAAKEAAAKEAAAKA, black] to the cationic antimicrobial peptide GW-H1 (residues 1–20, orange, 20 aa) at the C-terminus. The full continuous primary amino acid sequence is presented above the domain organization bar, indicating the deliberate insertion of the helical linker to minimize steric clashes, avoid domain entanglement, and preserve independent biological activities.

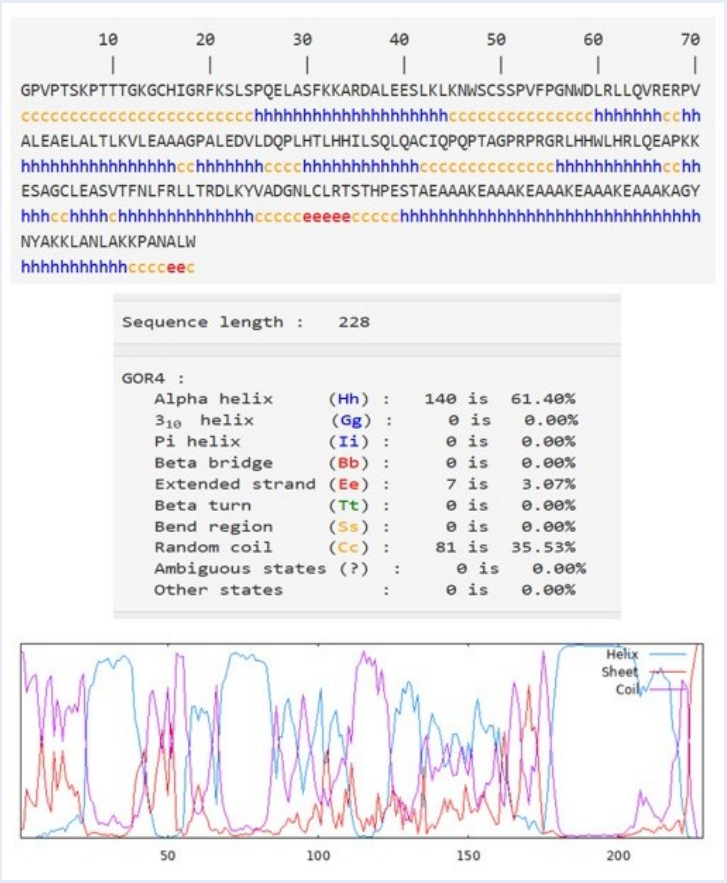

Figure 2: Secondary structure prediction of the chimeric IL-29–GW-H1 protein determined via GOR IV. Sequence-level and graphical representation of secondary structural elements predicted by the GOR IV web server for the 228-amino-acid chimeric construct. Top panel: amino acid sequence annotated with predicted conformational states, where 'h' (blue) denotes alpha-helical residues, 'e' (red) denotes extended beta-strands, and 'c' (orange) denotes random coil conformations. Middle panel: quantitative breakdown of structural elements, revealing 140 residues in alpha-helices (61.40%), 7 residues in extended beta-strands (3.07%), and 81 residues in random coils (35.53%). Bottom panel: continuous conformational probability profile across the entire sequence length, illustrating the high predominance of alpha-helical architecture that imparts structural stability to the fusion protein.

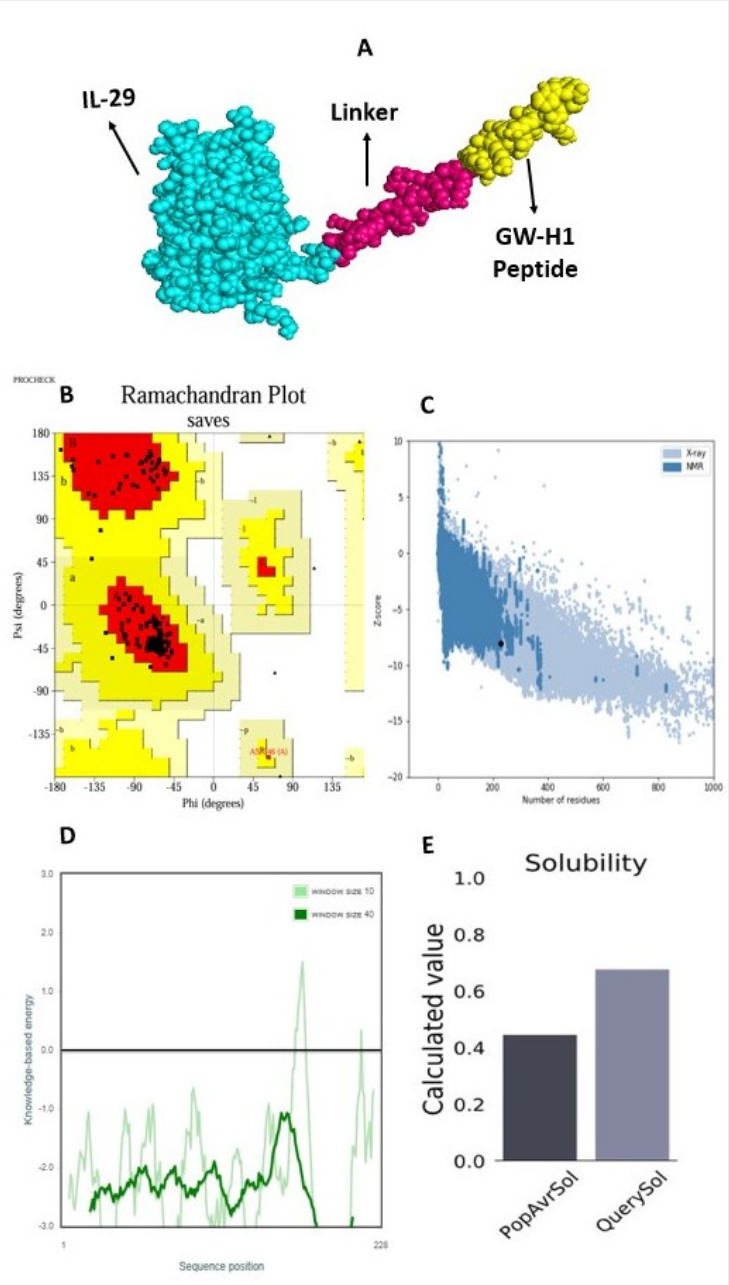

Figure 3: **Three-dimensional tertiary structure modeling, stereochemical validation, and aqueous solubility assessment of the chimeric IL-29–GW-H1 protein.** Structural validation and physicochemical evaluation of the optimized fusion construct. (A) 3D tertiary structure predicted by trRosetta and visualized in PyMOL, depicting the spatial orientation of IL-29 (cyan sphere model), the rigid alpha-helical linker (magenta sphere model), and the C-terminal GW-H1 peptide (yellow sphere model). (B) Ramachandran plot of the GalaxyRefine-optimized model generated using PROCHECK on the SAVES v6.0 server, demonstrating that 98.0% of non-glycine and non-proline residues reside in the most favored core regions [red], with zero residues in disallowed regions. (C) ProSA-web overall model quality plot displaying Z-score distributions of experimentally determined native protein structures from X-ray crystallography (light blue) and NMR spectroscopy (dark blue); the black dot represents the chimeric construct with a highly favorable Z-score of –8.09. (D) ProSA-web residue-by-residue knowledge-based energy profile calculated at sliding window sizes of 10 (light green) and 40 (dark green), exhibiting predominantly negative energy values across all 228 residues. (E) Aqueous solubility profile computed by the Protein-Sol server, comparing the population average solubility benchmark (PopAvrSol = 0.45) with the predicted query solubility score (QuerySol = 0.677), confirming high predicted solubility.

Table 2: Stereochemical quality comparison and structural validation metrics of three-dimensional (3D) models predicted by online computational servers.

3D Modeling Server	Residues in Most Favored RC Regions (%)	ERRAT Overall Quality Factor (%)	ProSA-web Z-score
trRosetta	96.0% (98.0% after GalaxyRefine)	95.15% (97.06% after GalaxyRefine)	–8.09
I-TASSER	82.0%	25.91%	–7.20
AlphaFold2 (ColabFold)	86.0%	79.82%	–8.22

Comparison of stereochemical parameters across trRosetta, I-TASSER, and AlphaFold2 predictions for the chimeric IL-29–GW-H1 protein. Validation was performed using the SAVES v6.0 server (PROCHECK for Ramachandran plot [RC] analysis, ERRAT for non-bonded atomic interaction quality factor) and ProSA-web for Z-score determination. The trRosetta model showed superior stereochemical parameters and was further improved via GalaxyRefine prior to receptor docking.

Table 3: Predicted physicochemical properties and structural parameters of the chimeric IL-29–GW-H1 construct.

Physicochemical Property	Analytical Value
Total number of amino acids	228 residues
Molecular weight (MW)	24,729.45 Da (24.7 kDa)
Theoretical isoelectric point (pI)	9.38 (basic)
Total number of negatively charged residues (Asp + Glu)	23
Total number of positively charged residues (Arg + Lys)	32
Total number of atoms	3,518
Estimated in vitro / in vivo half-life	30 hours (mammalian reticulocytes, in vitro) >20 hours (yeast, in vivo) >10 hours (*Escherichia coli*, in vivo)
Instability index (II)	45.32
Aliphatic index	86.71 (high thermostability)
Grand average of hydropathicity (GRAVY)	–0.365 (hydrophilic)
Molar extinction coefficient (at 280 nm in water)	26,720 M^{-1} cm^{-1}
Protein-Sol predicted solubility score	0.677 (soluble, threshold = 0.45)
SoluProt *E. coli* soluble expression score	0.955 (high soluble expression propensity)

Physicochemical parameters calculated via ExPASy ProtParam, Protein-Sol, and SoluProt servers based on the primary 228-amino-acid sequence of the chimeric IL-29–GW-H1 construct.

respectively). Cluster 0 was selected for detailed interfacial contact mapping and molecular dynamics simulations.

Protein-protein interaction profiling

Intermolecular interactions at the receptor-ligand interface were evaluated using PDBsum and PDBePISA (Figure 5). Analysis of the docked ternary complex revealed 8 salt bridges, 28 hydrogen bonds, and extensive non-bonded van der Waals contacts across the interface. At the IL-10Rβ (Chain A)–IL-29–GW-H1 (Chain C) interface, 11 hydrogen bonds were formed by residues Tyr42, Val3, His177, Arg43, Glu179, Thr9, Asn133, Asp92, Asp67, Lys7, and Cys89, alongside 4 salt bridges contributed by Arg43, Glu179, Asp92, and Lys7, and 64 non-bonded contacts. At the IL-28Rα (Chain B)–IL-29–GW-H1 (Chain C) interface, 14 hydrogen bonds were contributed by Ser175, Thr181, Arg46, His177, Lys75, Gly1, Arg173, Asp71, Tyr73, Asn169, Gln64, Gln70, Gln126, and Ala119, with 4 salt bridges formed by Glu53, Arg124, Asp71, and Arg173, and 107 non-bonded contacts. Binding free energy evaluation using the HawkDock MM/GBSA

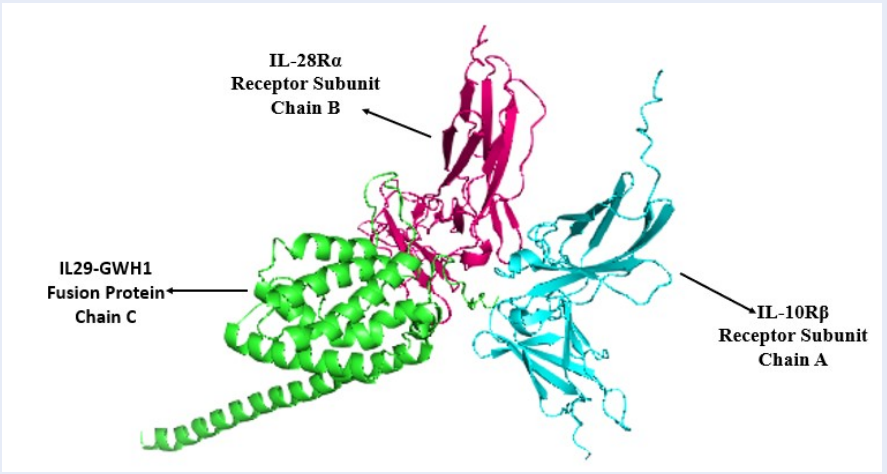

Figure 4: Molecular docking model of the chimeric IL-29–GW-H1 protein in complex with the IL-28Rα/IL-10Rβ heterodimeric receptor. 3D ribbon representation of the top-ranked docking complex (Cluster 0) generated by ClusPro 2.0 and rendered in PyMOL. The chimeric ligand IL-29–GW-H1 (Chain C, green ribbon) interacts simultaneously with the two subunits of the cognate receptor heterodimer: the IL-28Rα receptor subunit (Chain B, magenta ribbon) and the IL-10Rβ receptor subunit (Chain A, cyan ribbon). The binding conformation shows extensive interfacial contact and favorable structural complementarity across both receptor interfaces.

Table 4: Top 10 molecular docking clusters of the chimeric IL-29–GW-H1 protein in complex with the IL-28Rα/IL-10Rβ heterodimeric receptor generated by ClusPro 2.0.

Cluster Rank	Cluster Members	Representative Conformation	Weighted Energy Score (kcal/mol)	Lowest Energy Score (kcal/mol)
0	39	Center / Lowest Energy	−797.7	−839.8
1	33	Center / Lowest Energy	−744.0	−1031.6
2	31	Center / Lowest Energy	−756.4	−963.5
3	31	Center / Lowest Energy	−728.5	−836.4
4	28	Center / Lowest Energy	−779.0	−802.2
5	27	Center / Lowest Energy	−747.9	−897.6
6	26	Center / Lowest Energy	−820.4	−939.4
7	26	Center / Lowest Energy	−714.7	−926.0
8	25	Center / Lowest Energy	−712.8	−1045.8
9	22	Center / Lowest Energy	−805.5	−855.5
10	22	Center / Lowest Energy	−933.4	−933.4

Output parameters of protein-protein docking clusters for the IL-29–GW-H1 ligand against the IL-28Rα/IL-10Rβ heterodimer (PDB ID: 9BPU) using ClusPro 2.0. Cluster 0 had the highest cluster population (39 members) and a highly favorable energy score (−839.8 kcal/mol), representing the most reliable and consistent docking pose.

module yielded a favorable negative ΔG of −116.31 kcal/mol, while PRODIGY predicted a dissociation constant (K_d) of 3.8 × 10^{-11} M (ΔG = −14.2 kcal/mol), confirming high-affinity, stable receptor engagement.

Molecular dynamics simulations and essential dynamics

To evaluate the structural stability, conformational compactness, and dynamic behavior of the IL-29–GW-H1–IL-28Rα–IL-10Rβ complex under physiological conditions, a 100 ns all-atom MD simulation was performed (Figures 6 and 7). Residue-level root mean square fluctuation (RMSF) analysis showed that the majority of residues exhibited low fluctuations (1–4 Å), reflecting conformational rigidity in core secondary structures and the receptor-binding interface (Figure 6B). Elevated fluctuations were confined to solvent-exposed terminal residues and loop regions around residues 200 and 410. Back-

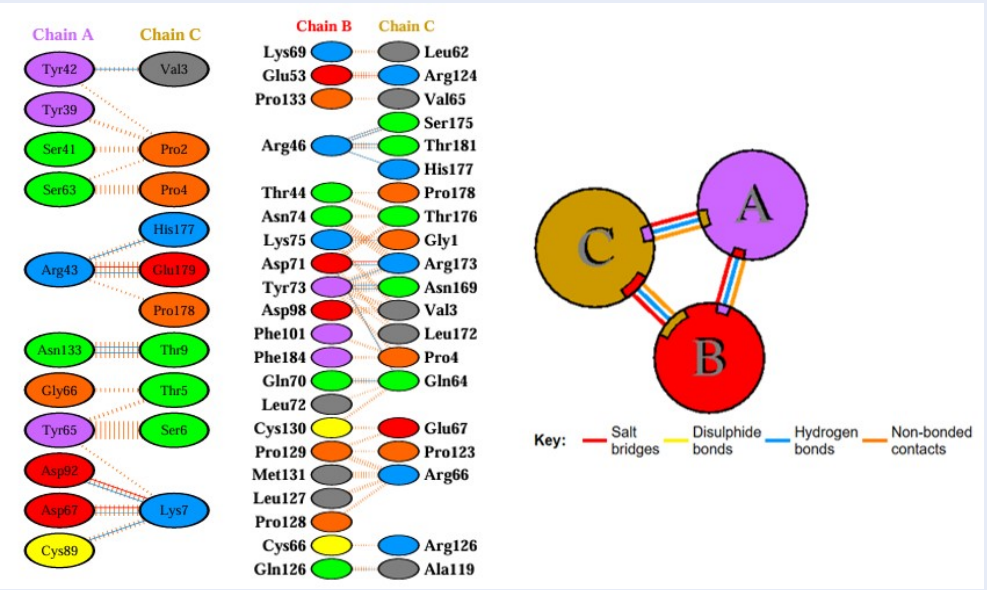

Figure 5: Detailed interfacial contact network and molecular interactions within the IL-29–GW-H1–IL-28Rα–IL-10Rβ receptor complex. 2D interaction map of amino acid contacts at the protein-protein interfaces generated by PDBsum and PDBePISA. Left panel: residue-specific interactions between the IL-10Rβ receptor subunit (Chain A, purple) and the chimeric IL-29–GW-H1 ligand (Chain C, orange/green/grey), mediated by 11 hydrogen bonds (blue dashed lines), 4 salt bridges (red solid lines), and 64 non-bonded van der Waals contacts (orange striped lines). Middle panel: residue-specific interactions between the IL-28Rα receptor subunit (Chain B, red) and the chimeric ligand (Chain C), mediated by 14 hydrogen bonds, 4 salt bridges, and 107 non-bonded contacts. Right panel: schematic inter-chain network diagram illustrating the synergistic multipoint binding architecture and salt bridge stabilization among Chains A, B, and C.

bone root mean square deviation (RMSD) increased during the initial 0–15 ns equilibration phase as the static docked pose relaxed in solvent, after which it stabilized into a steady plateau fluctuating between 10 and 13 Å throughout the remainder of the 100 ns trajectory (Figure 6C). The radius of gyration (Rg) remained tightly constrained between 31.5 and 32.5 Å (Figure 6A), indicating that the complex preserved its compact tertiary fold without unfolding. Structural superposition of snapshots at 0 ns (blue), 50 ns (green), and 100 ns (red) confirmed that global domain rearrangements were minimal once equilibrium was reached (Figure 6D).

Dynamic cross-correlation matrix (DCCM) analysis revealed dominant regions of positive correlation across receptor domains and at the ligand-receptor interface (Figure 7B), demonstrating synchronized domain dynamics necessary for signaling complex stability. Principal component analysis (PCA) scatter plotting showed that conformational sampling along PC1 and PC2 clustered predominantly in low-energy regions (Figure 7A). The 3D Free Energy Landscape (FEL) constructed from PC1 and PC2 exhibited a single, deep global energy minimum basin surrounded by shallow local basins (Figure 7C), confirming that the docked complex resides in a thermodynamically stable state throughout the simulation trajectory.

Cloning and recombinant expression of the chimeric IL29-GWH1 gene

The synthetic IL-29 and chimeric IL-29–GW-H1 genes were successfully cloned into the pET29b(+) expression vector under the control of the T7 promoter (Figure 8B). Restriction endonuclease digestion and PCR amplification confirmed the presence of the expected 684 bp insert (Figure 8A). The recombinant plasmids were transformed into *E. coli* BL21(DE3) for protein expression.

Fermentation, solubilization, and refolding

Shake-flask fermentations yielded 7.5 g/L and 8.0 g/L of wet cell biomass for wild-type IL-29 and chimeric IL-29–GW-H1, respectively. Following cell lysis via French press at 1.5 kbar, inclusion bodies (IBs) were recovered at 3.2 g/L (IL-29) and 3.0

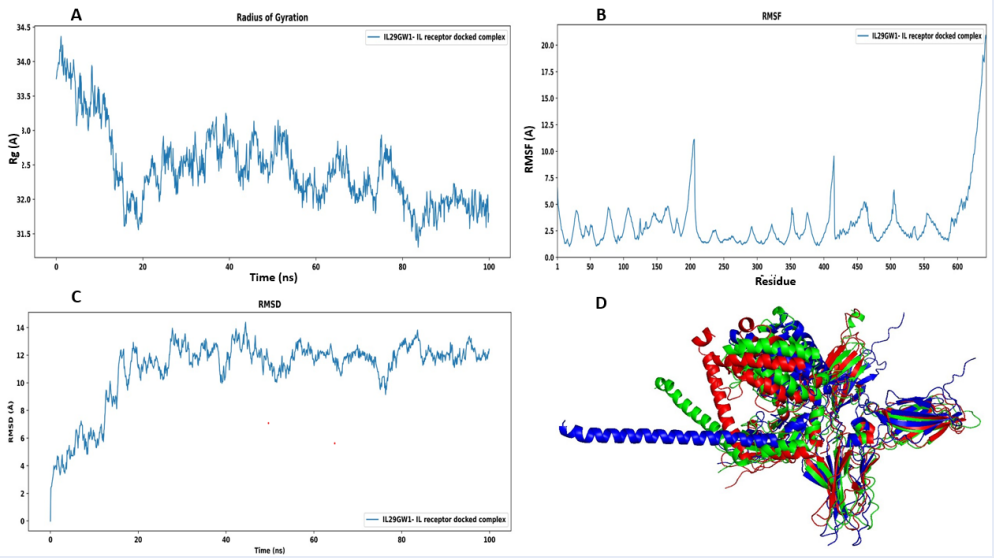

Figure 6: All-atom molecular dynamics (MD) simulation trajectory analysis of the IL-29–GW-H1–receptor complex over 100 ns. Dynamic stability and conformational trajectory analysis of the docked IL-29–GW-H1–IL-28Rα–IL-10Rβ ternary complex simulated in Desmond (Schrödinger) for 100 ns under physiological conditions (310 K, 1.0 atm, 0.15 M NaCl). (A) Radius of gyration (Rg) plot over the 100 ns trajectory, showing rapid structural compaction and tight maintenance within 31.5–32.5 Å. (B) Residue-wise root mean square fluctuation (RMSF) profile across the 635 total residues of the complex, showing low baseline fluctuations (1–4 Å) in core alpha-helices and binding interfaces, with localized peaks restricted to flexible loop regions (near residues 200 and 410) and solvent-exposed termini. (C) Backbone root mean square deviation (RMSD) plot of the complex relative to the initial docking pose, showing initial solvent relaxation during 0–15 ns followed by a stable equilibrium plateau fluctuating between 10 and 13 Å throughout the remaining 85 ns. (D) 3D structural superposition of the complex captured at 0 ns (initial docked pose, blue), 50 ns (intermediate pose, green), and 100 ns (final simulation pose, red), confirming that the overall ternary fold and receptor-ligand interface remain stably intact without complex dissociation.

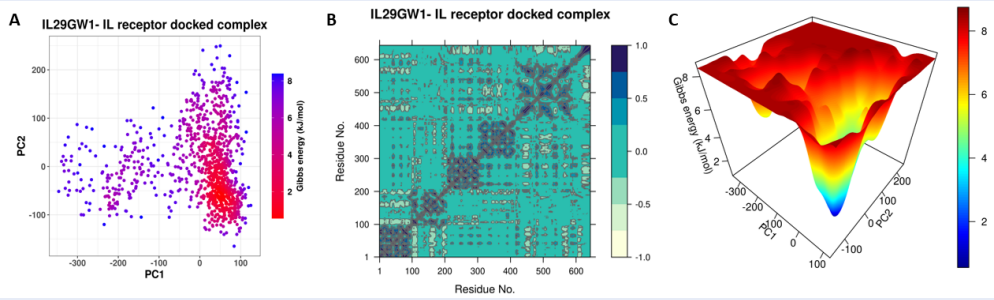

Figure 7: Essential dynamics, dynamic cross-correlation matrix (DCCM), and 3D free energy landscape (FEL) of the docked ternary complex. Conformational sampling and energetic landscape of the IL-29–GW-H1–IL-28Rα–IL-10Rβ complex during 100 ns MD simulation. (A) Principal component analysis (PCA) 2D scatter plot projecting conformational trajectories onto the first two principal components (PC1 vs. PC2), color-coded by Gibbs free energy (kJ/mol) from low energy (red) to higher energy (purple). (B) Dynamic cross-correlation matrix (DCCM) showing correlated atomic motions (positive values, dark blue/cyan) and anti-correlated motions (negative values, light yellow) across all residue pairs, indicating strong cooperative movements at the ligand-receptor binding interface. (C) 3D Free Energy Landscape (FEL) constructed as a function of PC1 and PC2, showing a single deep, well-defined global energy minimum basin that confirms the thermodynamic stability and conformational convergence of the engineered chimeric complex under simulated biological conditions.

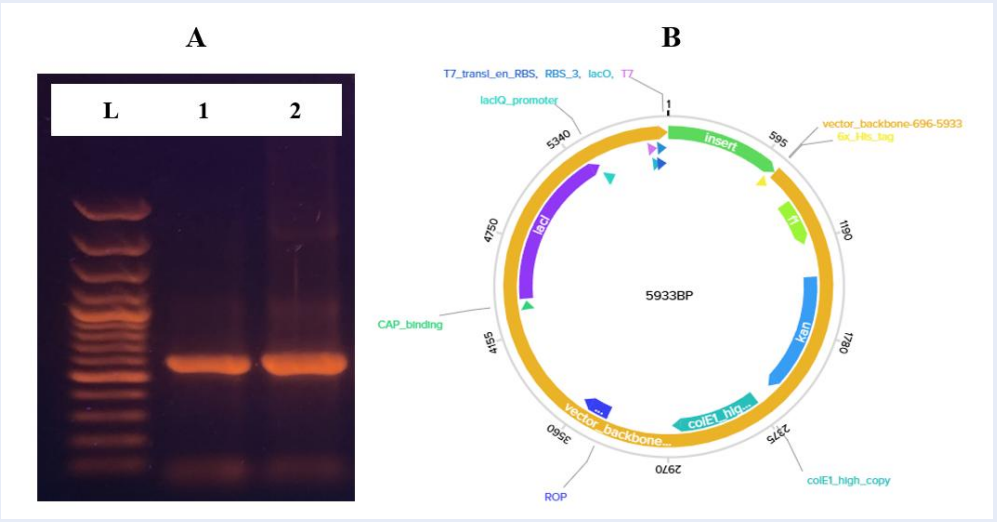

Figure 8: **Construction of the recombinant expression vector and PCR validation of the chimeric IL-29–GW-H1 gene.** Molecular cloning of the target construct into the bacterial expression host. (A) 1.2% agarose gel electrophoresis of the PCR-amplified chimeric gene product (Lane L: DNA ladder; Lanes 1–2: verified 684 bp amplicon encoding IL-29–GW-H1). (B) Circular plasmid map of the recombinant pET29b(+) expression vector (5,933 bp) containing the cloned IL-29–GW-H1 insert between *Nde*I and *Xho*I restriction sites under the control of the T7 promoter, featuring a C-terminal 6×His tag for affinity purification, kanamycin resistance marker (*kan*), and *lacI* repressor gene.

g/L (IL-29–GW-H1). Solubilization in 6 M guanidine hydrochloride followed by controlled dilution in L-arginine-containing refolding buffer facilitated efficient protein renaturation (Table 5).

Affinity purification and electrophoretic characterization

Refolded IL-29 and IL-29–GW-H1 proteins were purified using Ni-NTA affinity chromatography on an ÄKTA Explorer FPLC system (Figure 9C). Wild-type IL-29 was recovered at a purified yield of 71 ± 1.0 mg/L (overall yield: 25.6 ± 1.0%), and chimeric IL-29–GW-H1 was recovered at 63 ± 1.0 mg/L (overall yield: 22.2 ± 1.0%) (Table 5). SDS-PAGE analysis revealed single homogeneous bands at their expected molecular weights (20 kDa for wild-type IL-29 and 24 kDa for IL-29–GW-H1), confirming a purity exceeding 98% (Figure 9A). Western blot analysis using anti-6×His antibodies confirmed target protein identity (Figure 9B).

In vitro cytotoxicity against HepG2 and HEK293 cells

The cytotoxic activities of purified IL-29 and chimeric IL-29–GW-H1 were evaluated against HepG2 hepatoma cells and non-tumorigenic HEK293 embryonic kidney cells using the MTT assay (Figure 10). Both proteins demonstrated concentration-dependent inhibition of HepG2 cell viability over 24 h (Figure 10A, B). The chimeric IL-29–GW-H1 protein exhibited significantly enhanced cytotoxic potency against HepG2 cells compared to wild-type IL-29, with a lower half-maximal inhibitory concentration (IC_{50} = 16.31 μg/mL vs. 20.14 μg/mL; $p < 0.001$). When tested against normal HEK293 cells (Figure 10C), both proteins demonstrated low toxicity: cell viability remained between 70% and 98% across concentrations of 5–20 μg/mL, and more than 60% of HEK293 cells remained viable even at the maximum concentration of 25 μg/mL. These results indicate that the chimeric IL-29–GW-H1 construct achieves superior antitumor efficacy against hepatocellular carcinoma cells while sparing non-malignant cells.

DISCUSSION

A primary goal in cancer pharmacotherapy is the development of therapeutic agents that selectively eliminate malignant cells while preserving healthy tissues. Conventional mono-therapeutic options—including systemic chemotherapy, radiation, and non-targeted small molecules—are frequently compromised by off-target toxicities, rapid metabolic clearance, and the emergence of drug resistance[39,40]. Furthermore, standard chemothera-

Table 5: Quantitative yields and recovery metrics during expression, refolding, and Ni-NTA chromatographic purification of wild-type IL-29 and chimeric IL-29–GW-H1.

Recombinant Construct	Wet Cell Biomass (g/L)	Inclusion Bodies (a) (g/L)	Total Protein (b) (mg/L)	Refolded & Diafiltered Protein (c) (mg/L)	Purified Protein (d) (mg/L)	Overall Purification Yield* (e) (%)
Wild-type IL-29	7.5 ± 0.3	3.2 ± 0.2	277 ± 5.0	220 ± 5.0	71 ± 1.0	25.6 ± 1.0%
Chimeric IL-29–GW-H1	8.0 ± 0.4	3.0 ± 0.1	284 ± 5.0	221 ± 5.0	63 ± 1.0	22.2 ± 1.0%

Stepwise recovery and yield analysis of recombinant proteins produced from 1.0 L batch shake-flask fermentations in *E. coli* BL21(DE3). Values represent the mean ± SD of three independent purification runs (n = 3). *Formula for overall yield calculation: Overall Yield (%) = [Purified protein (mg/L) / Total protein (mg/L)] × 100.

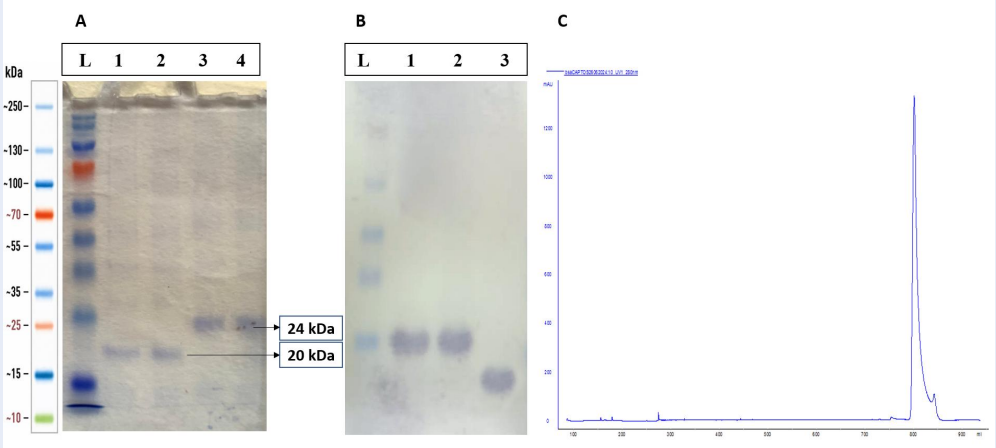

Figure 9: Chromatographic purification, electrophoretic verification, and immunoblotting of recombinant wild-type IL-29 and chimeric IL-29–GW-H1 proteins. Purification and biochemical characterization of refolded recombinant proteins. (A) 12% SDS-PAGE analysis stained with Coomassie Brilliant Blue R-250 (Lane L: pre-stained protein molecular weight ladder; Lanes 1–2: purified wild-type IL-29 resolving at 20 kDa; Lanes 3–4: purified chimeric IL-29–GW-H1 resolving at 24 kDa), demonstrating >98% protein purity. (B) Western blot analysis using mouse anti-6×His primary monoclonal antibody and HRP-conjugated secondary antibody, visualized with NBT/BCIP substrate (Lane L: pre-stained ladder; Lanes 1–2: purified chimeric IL-29–GW-H1 at 24 kDa; Lane 3: purified wild-type IL-29 at 20 kDa). (C) Fast protein liquid chromatography (FPLC) Ni-NTA affinity elution chromatogram (ÄKTA Explorer) showing the sharp target protein absorbance peak at 280 nm (blue trace) upon elution with 0.5 M imidazole.

peutics often fail to target quiescent or slow-cycling cancer cells and may increase the risk of secondary malignancies[40]. Recombinant chimeric proteins engineered by joining cytokine domains to tumor-targeting or cell-lytic peptides offer a compelling strategy to overcome these limitations by enhancing tumor receptor specificity, delivering localized cytotoxicity, and reducing systemic side effects[7,10,11].

In this study, human Interleukin-29 was fused to the synthetic cationic antimicrobial peptide GW-H1 via a rigid alpha-helical linker [A(EAAAK)$_5$A]. The rigid linker was selected because helical linkers effectively separate functional domains, minimize steric clash, prevent domain-domain entanglement, and preserve the independent folding and bioactivity of each partner[21,22]. Tertiary structure prediction using trRosetta yielded a highly reliable 3D model with a TM-score of 0.829, which was further optimized by GalaxyRefine. Stereochemical evaluation demonstrated that 98.0% of residues resided in favored Ramachandran regions, with an ERRAT overall quality factor of 97.06% and a ProSA Z-score of –8.09, confirming native-like structural validity[12,25,26,38]. Physicochemical profiling revealed an aliphatic index of 86.71, supporting thermal stability, and a negative GRAVY score (–0.365), indicating hydrophilicity and aqueous solubility, consistent with Protein-Sol and SoluProt predictions[27,30,31].

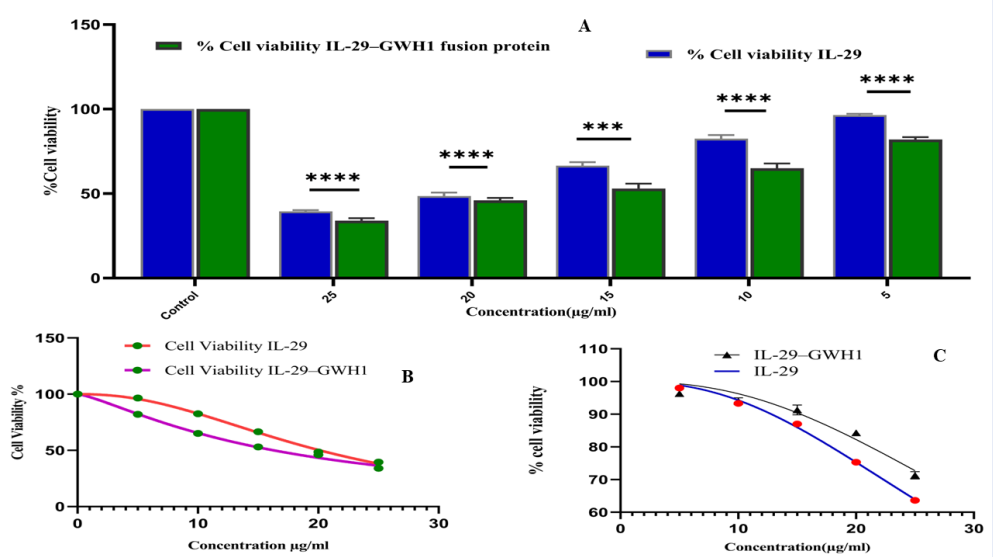

Figure 10: **In vitro cytotoxicity and selectivity profiling of wild-type IL-29 and chimeric IL-29–GW-H1 against HepG2 and HEK293 cells.** Concentration-dependent cell viability assessed by MTT colorimetric assay following 24 h exposure to varying concentrations (5–25 µg/mL). (A) Comparative bar graph of HepG2 hepatocellular carcinoma cell viability after treatment with wild-type IL-29 (blue bars) versus chimeric IL-29–GW-H1 (green bars) relative to untreated control cells. (B) Dose-response cytotoxicity curves in HepG2 cells, illustrating a significantly lower IC_{50} for chimeric IL-29–GW-H1 (16.31 µg/mL) compared to wild-type IL-29 (20.14 µg/mL). (C) Cell viability profile of non-tumorigenic human embryonic kidney cells (HEK293) treated with wild-type IL-29 (blue line/red circles) and chimeric IL-29–GW-H1 (black line/triangles), showing high cell viability (70–98% across 5–20 µg/mL and >60% at 25 µg/mL), indicative of low off-target toxicity on non-malignant cells. All data represent the mean ± standard deviation (SD) of three independent experiments performed in triplicate ($n = 3$). Asterisks denote statistically significant differences between IL-29 and IL-29–GW-H1 treatments at each respective concentration (**$p < 0.01$, ***$p < 0.001$, ****$p < 0.0001$; one-way ANOVA followed by Tukey's post-hoc test).

Molecular docking via ClusPro 2.0 and interaction profiling revealed that the chimeric construct binds with high affinity to the IL-28Rα/IL-10Rβ heterodimeric receptor complex[32,33]. The top-ranked docking pose was stabilized by 8 salt bridges and 28 hydrogen bonds distributed across both receptor subunits, yielding an MM/GBSA binding free energy of −116.31 kcal/mol and a predicted K_d of 3.8×10^{-11} M[34,43–45]. Molecular dynamics simulations over 100 ns demonstrated that the ternary complex achieved stable equilibration within 15 ns, maintained low residue fluctuations in core regions (RMSF 1–4 Å), and exhibited a tightly constrained radius of gyration (31.5–32.5 Å)[35,36]. Dynamic cross-correlation and free energy landscape analyses confirmed cooperative interfacial dynamics and convergence into a single, deep global energy minimum basin, validating the thermodynamic stability of the engineered complex under physiological conditions.

Recombinant protein expression in *Escherichia coli* BL21(DE3) resulted in robust accumulation of target proteins in inclusion bodies, which were successfully solubilized in guanidine hydrochloride and refolded using an optimized L-arginine-assisted dilution protocol[46,47]. Single-step Ni-NTA affinity chromatography yielded high-purity (>98%) recombinant proteins (71 mg/L for IL-29 and 63 mg/L for IL-29–GW-H1)[37,48,49]. In vitro functional evaluation against HepG2 hepatoma cells demonstrated that the chimeric IL-29–GW-H1 protein possessed significantly higher cytotoxic activity (IC_{50} = 16.31 µg/mL) than wild-type IL-29 (IC_{50} = 20.14 µg/mL; $p < 0.001$). This enhanced potency reflects the synergistic combination of IL-29-mediated receptor activation with the membrane-disruptive and caspase-dependent apoptotic actions of the GW-H1 peptide[20,50]. Importantly, when tested against non-tumorigenic HEK293 cells, both IL-29 and the chimeric construct exhibited low cytotoxicity, maintaining >60% viability at the highest tested dose (25 µg/mL), thereby supporting the tumor selectivity of the construct.

Although these findings demonstrate the therapeutic promise of the chimeric IL-29–GW-H1 pro-

tein, several limitations should be acknowledged. First, the biological evaluations were conducted in vitro using established 2D cell cultures. Future studies will need to evaluate the construct in 3D spheroid models, patient-derived primary hepatocytes, and in vivo orthotopic HCC animal models to characterize its pharmacokinetic, biodistribution, and toxicology profiles. Second, while bacterial expression in *E. coli* yielded high protein quantities, expression in mammalian or yeast host systems should be explored to assess the influence of post-translational modifications (such as N-glycosylation) on in vivo stability and immunogenicity. Third, routine short tandem repeat (STR) authentication and mycoplasma screening should be implemented in subsequent preclinical studies to reinforce data rigor. Nonetheless, the computational and experimental data presented here establish IL-29–GW-H1 as a structurally stable and potent chimeric biotherapeutic candidate for targeted liver cancer therapy.

CONCLUSION

In this study, a novel bifunctional chimeric protein combining human Interleukin-29 with the cationic antimicrobial peptide GW-H1 was successfully designed, modeled, and experimentally validated. Computational modeling, molecular docking, and 100 ns molecular dynamics simulations demonstrated that the chimeric construct forms a stable, high-affinity complex with the IL-28Rα/IL-10Rβ heterodimeric receptor. The recombinant fusion protein was efficiently expressed in *E. coli*, refolded from inclusion bodies, and purified to >98% purity. In vitro MTT assays demonstrated that the chimeric IL-29–GW-H1 protein exhibits superior cytotoxic efficacy against HepG2 hepatocellular carcinoma cells compared to wild-type IL-29 while maintaining minimal toxicity against non-malignant HEK293 cells. These findings highlight the potential of IL-29–GW-H1 as a targeted immunotherapeutic agent for liver cancer and provide a foundation for future in vivo preclinical development.

DECLARATIONS

Abbreviations

3D: Three-dimensional; **ANOVA:** Analysis of variance; **ATCC:** American Type Culture Collection; **DCCM:** Dynamic cross-correlation matrix; **DMEM:** Dulbecco's Modified Eagle's Medium; **DMSO:** Dimethyl sulfoxide; ***E. coli*:** *Escherichia coli*; **EDTA:** Ethylenediaminetetraacetic acid; **ERRAT:** Empirical structure quality factor; **FBS:** Fetal bovine serum; **FEL:** Free energy landscape; **FPLC:** Fast protein liquid chromatography; **GOR:** Garnier-Osguthorpe-Robson secondary structure prediction; **GRAVY:** Grand average of hydropathicity; **GW-H1:** Cationic antimicrobial peptide (20 aa); **HCC:** Hepatocellular carcinoma; **HRP:** Horseradish peroxidase; **HSD:** Honestly significant difference; **IBs:** Inclusion bodies; **IC_{50}:** Half-maximal inhibitory concentration; **IFN:** Interferon; **IFN-λ:** Interferon-lambda; **IL-10Rβ:** Interleukin-10 receptor subunit beta; **IL-28Rα:** Interleukin-28 receptor subunit alpha; **IL-29:** Interleukin-29; **IMAC:** Immobilized metal affinity chromatography; **IPTG:** Isopropyl β-D-1-thiogalactopyranoside; **IRF9:** Interferon regulatory factor 9; **ISGF3:** Interferon-stimulated gene factor 3; **ISRE:** Interferon-stimulated response element; **JAK-STAT:** Janus kinase/signal transducer and activator of transcription; **K_d:** Dissociation constant; **kDa:** Kilodalton; **MD:** Molecular dynamics; **MM/GBSA:** Molecular mechanics generalized Born surface area; **MTT:** 3-(4,5-Dimethylthiazol-2-yl)-2,5-diphenyltetrazolium bromide; **MW:** Molecular weight; **NBT/BCIP:** Nitro-blue tetrazolium / 5-bromo-4-chloro-3'-indolyl phosphate; **NCBI:** National Center for Biotechnology Information; **Ni-NTA:** Nickel-nitrilotriacetic acid; **OD_{600}:** Optical density at 600 nm; **PBS:** Phosphate-buffered saline; **PCA:** Principal component analysis; **PDB:** Protein Data Bank; **pI:** Isoelectric point; **PMSF:** Phenylmethylsulfonyl fluoride; **RC:** Ramachandran plot; **Rg:** Radius of gyration; **RMSD:** Root mean square deviation; **RMSF:** Root mean square fluctuation; **rpm:** Revolutions per minute; **SAVES:** Structural Analysis and Verification Server; **SD:** Standard deviation; **SDS-PAGE:** Sodium dodecyl sulfate polyacrylamide gel electrophoresis; **TB:** Terrific Broth; **TBST:** Tris-buffered saline with Tween-20; **TM-score:** Template modeling score.

Acknowledgments

The authors express their sincere gratitude to all individuals, researchers, and technical staff at the Centre for Applied Molecular Biology (CAMB), the School of Biochemistry and Biotechnology, and the Centre of Excellence in Molecular Biology (CEMB), University of the Punjab, as well as the University of Lahore, for providing laboratory infrastructure, technical assistance, academic guidance, and constructive scientific discussions that contributed to this research.

Author's contributions

HMR and **HB** conceived and designed the study. **HMR**, **ON**, **HMR (Hafiz Muzzammel Rehman)**, and **NA** performed the in silico computational modeling, molecular docking, and molecular dynamics simulations. **HMR**, **IG**, **AA**, **TR**, **AAs (Ariba Asif)**, and **HK** conducted recombinant gene cloning, bacterial fermentation, protein refolding, and Ni-NTA chromatographic purification. **HMR**, **AA**, **TR**, and **HB** performed the SDS-PAGE, Western blotting, and in vitro MTT cytotoxicity assays. **HMR**, **ON**, **NA**, and **HB** analyzed and interpreted the data. **HMR**, **ON**, and **HB** drafted the original manuscript. All authors critically reviewed, edited, and approved the final version of the manuscript.

Funding

None. The authors declare that no specific grants or financial support were received from any funding agency in the public, commercial, or not-for-profit sectors for this research.

Availability of data and materials

All data generated or analyzed during this study, including structural models, docking coordinates, and cytotoxicity values, are included in this published article. Additional primary datasets are available from the corresponding author upon reasonable request.

Ethics approval and consent to participate

Not applicable. This study did not involve human participants, clinical trials, or live vertebrate animals; all experimental procedures were performed using established commercial cell lines (HepG2 and HEK293) and computational simulations.

Consent for publication

Not applicable.

Declaration of generative AI and AI-assisted technologies in the writing process

None. The authors declare that no generative artificial intelligence (AI) or AI-assisted technologies were utilized in the writing, data analysis, or manuscript preparation process.

Competing interests

The authors declare that they have no competing interests, financial or otherwise, that could be perceived as influencing the work reported in this manuscript.

REFERENCES

1. Hassanpour SH, Dehghani M. Review of cancer from perspective of molecular. Journal of Cancer Research and Practice. 2017;4(4):127–129. Available from: https://doi.org/10.1016/j.jcrpr.2017.07.001.
2. Koul B. Types of cancer. Herbs for Cancer Treatment. Singapore: Springer; 2020.
3. Siegel RL, Miller KD, Jemal A. Cancer statistics, 2016. CA: A Cancer Journal for Clinicians. 2016;66(1):7–30. PMID: 26742998. Available from: https://doi.org/10.3322/caac.21332.
4. Ferlay J, Shin HR, Bray F, Forman D, Mathers C, Parkin DM. Estimates of worldwide burden of cancer in 2008: GLOBOCAN 2008. International Journal of Cancer. 2010 Dec;127(12):2893–2917. PMID: 21351269. Available from: https://doi.org/10.1002/ijc.25516.
5. Rehman HM, Naz M, Ghous AG, Malik M, Ahmad S, Bashir H. Computational design and evaluation of a novel temporin 1CEa-IL24 fusion protein for anti-tumor potential. Biomedical Research and Therapy. 2025;12(2):7138–7152. Available from: https://doi.org/10.15419/bmrat.v12i2.959.
6. Aslam S, Rehman HM, Sarwar MZ, Ahmad A, Ahmed N, Amirzada MI, et al. Computational Modeling, High-Level Soluble Expression and In Vitro Cytotoxicity Assessment of Recombinant Pseudomonas aeruginosa Azurin: A Promising Anti-Cancer Therapeutic Candidate. Pharmaceutics. 2023 Jun;15(7):1825. PMID: 37514012. Available from: https://doi.org/10.3390/pharmaceutics15071825.
7. Qureshi S, Ahmed N, Rehman HM, Amirzada MI, Saleem F, Waheed K, et al. Investigation of therapeutic potential of the Il24-p20 fusion protein against breast cancer: an in-silico approach. In Silico Pharmacology. 2024 Sep;12(2):84. PMID: 39301086. Available from: https://doi.org/10.1007/s40203-024-00252-x.
8. Smith LL, Brown K, Carthew P, Lim CK, Martin EA, Styles J, et al. Chemoprevention of breast cancer by tamoxifen: risks and opportunities. Critical Reviews in Toxicology. 2000 Sep;30(5):571–594. PMID: 11055836. Available from: https://doi.org/10.1080/10408440008951120.
9. Fatima T, Mubasher MM, Rehman HM, Niyazi S, Alanzi AR, Kalsoom M, et al. Computational modeling study of IL-15-NGR peptide fusion protein: a targeted therapeutics for hepatocellular carcinoma. AMB Express. 2024 Aug;14(1):91. PMID: 39133343. Available from: https://doi.org/10.1186/s13568-024-01747-8.
10. Aroul-Selvam R, Hubbard T, Sasidharan R. Domain insertions in protein structures. Journal of Molecular Biology. 2004 May;338(4):633–641. PMID: 15099733. Available from: https://doi.org/10.1016/j.jmb.2004.03.039.
11. Yu K, Liu C, Kim BG, Lee DY. Synthetic fusion protein design and applications. Biotechnology Advances. 2015;33(1):155–164. PMID: 25450191. Available from: https://doi.org/10.1016/j.biotechadv.2014.11.005.
12. Muhammad Rehman H, Rehman HM, Naveed M, Khan MT, Shabbir MA, Aslam S, et al. In Silico investigation of a chimeric IL24-LK6 fusion protein as a potent candidate against breast cancer. Bioinformatics and Biology Insights. 2023 Jun;17:11779322231182560. PMID: 37377793. Available from: https://doi.org/10.1177/11779322231182560.
13. Rehman HM, Rehman HM, Ahmed N, Imran M. In silico design and evaluation of Novel Cell Targeting Melittin-Interleukin-24 Fusion protein: a potential drug candidate against breast Cancer. Sains Malaysiana. 2023;52(11):3223–3237. Available from: https://doi.org/10.17576/jsm-2023-5211-15.
14. Smyth MJ, Cretney E, Kershaw MH, Hayakawa Y. Cytokines in cancer immunity and immunotherapy. Immunological Reviews. 2004 Dec;202(1):275–293. PMID: 15546400. Available from: https://doi.org/10.1111/j.0105-2896.2004.00199.x.
15. Kotenko SV, Gallagher G, Baurin VV, Lewis-Antes A, Shen M, Shah NK, et al. IFN-lambdas mediate antiviral protection through a distinct class II cytokine receptor complex. Nature Immunology. 2003 Jan;4(1):69–77. PMID: 12483210. Available

from: https://doi.org/10.1038/ni875.
16. Donnelly RP, Kotenko SV. Interferon-lambda: a new addition to an old family. Journal of Interferon & Cytokine Research. 2010 Aug;30(8):555–564. PMID: 20712453. Available from: https://doi.org/10.1089/jir.2010.0078.
17. Doyle SE, Schreckhise H, Khuu-Duong K, Henderson K, Rosler R, Storey H, et al. Interleukin-29 uses a type 1 interferon-like program to promote antiviral responses in human hepatocytes. Hepatology. 2006 Oct;44(4):896–906. PMID: 17006906. Available from: https://doi.org/10.1002/hep.21312.
18. Maher SG, Sheikh F, Scarzello AJ, Romero-Weaver AL, Baker DP, Donnelly RP, et al. IFNalpha and IFNlambda differ in their antiproliferative effects and duration of JAK/STAT signaling activity. Cancer Biology & Therapy. 2008 Jul;7(7):1109–1115. PMID: 18698163. Available from: https://doi.org/10.4161/cbt.7.7.6192.
19. Serna N, Sánchez-García L, Sánchez-Chardi A, Unzueta U, Roldán M, Mangues R, et al. Protein-only, antimicrobial peptide-containing recombinant nanoparticles with inherent built-in antibacterial activity. Acta Biomaterialia. 2017 Sep;60:256–263. PMID: 28735028. Available from: https://doi.org/10.1016/j.actbio.2017.07.027.
20. Chen YL, Li JH, Yu CY, Lin CJ, Chiu PH, Chen PW, et al. Novel cationic antimicrobial peptide GW-H1 induced caspase-dependent apoptosis of hepatocellular carcinoma cell lines. Peptides. 2012 Aug;36(2):257–265. PMID: 22659412. Available from: https://doi.org/10.1016/j.peptides.2012.05.011.
21. Chen X, Zaro JL, Shen WC. Fusion protein linkers: property, design and functionality. Advanced Drug Delivery Reviews. 2013 Oct;65(10):1357–1369. PMID: 23026637. Available from: https://doi.org/10.1016/j.addr.2012.09.039.
22. Arai R, Ueda H, Kitayama A, Kamiya N, Nagamune T. Design of the linkers which effectively separate domains of a bifunctional fusion protein. Protein Engineering. 2001 Aug;14(8):529–532. PMID: 11579220. Available from: https://doi.org/10.1093/protein/14.8.529.
23. Garnier J, Gibrat JF, Robson B. GOR method for predicting protein secondary structure from amino acid sequence. Methods in Enzymology. 1996;266:540–553. PMID: 8743705. Available from: https://doi.org/10.1016/S0076-6879(96)66034-0.
24. Mohseni Moghadam Z, Halabian R, Sedighian H, Behzadi E, Amani J, Imani Fooladi AA. Designing and analyzing the structure of DT-STXB fusion protein as an anti-tumor agent: an in silico approach. Iranian Journal of Pathology. 2019;14(4):305–312. PMID: 31754360. Available from: https://doi.org/10.30699/IJP.2019.101200.2004.
25. Pourhadi M, Jamalzade F, Jahanian-Najafabadi A, Shafiee F. Expression, purification, and cytotoxic evaluation of IL24-BR2 fusion protein. Research in Pharmaceutical Sciences. 2019 Aug;14(4):320–328. PMID: 31516508. Available from: https://doi.org/10.4103/1735-5362.263556.
26. Javaid MS, Kaul H, Fazal N, Yaqub F, Naseer N, Hanif M, et al. In silico analysis to reveal underlying trans differentiation mechanism of Mesenchymal Stem Cells into Osteocytes. Advanced Life Sciences. 2021;8(4):412–418. Available from: https://doi.org/10.62940/als.v8i4.1297.
27. Gasteiger E, Hoogland C, Gattiker A, Duvaud S, Wilkins MR, Appel RD, et al. Protein identification and analysis tools on the ExPASy server. The Proteomics Protocols Handbook. Totowa (NJ): Humana Press; 2005. Available from: https://doi.org/10.1385/1-59259-890-0:571.
28. Doytchinova IA, Flower DR. VaxiJen: a server for prediction of protective antigens, tumour antigens and subunit vaccines. BMC Bioinformatics. 2007 Jan;8(1):4. PMID: 17207271. Available from: https://doi.org/10.1186/1471-2105-8-4.
29. Dimitrov I, Flower DR, Doytchinova I. AllerTOP—a server for in silico prediction of allergens. BMC Bioinformatics. 2013;14(Suppl 6):S4. PMID: 23735058. Available from: https://doi.org/10.1186/1471-2105-14-S6-S4.
30. Pimtawong T, Ren J, Lee J, Lee HM, Na D. A review on computational models for predicting protein solubility. Journal of Microbiology. 2025 Jan;63(1):2408001. PMID: 39895070. Available from: https://doi.org/10.71150/jm.2408001.
31. Hon J, Marusiak M, Martinek T, Kunka A, Zendulka J, Bednar D, et al. SoluProt: prediction of soluble protein expression in Escherichia coli. Bioinformatics. 2021 Apr;37(1):23–28. PMID: 33416864. Available from: https://doi.org/10.1093/bioinformatics/btaa1102.
32. Kozakov D, Hall DR, Xia B, Porter KA, Padhorny D, Yueh C, et al. The ClusPro web server for protein-protein docking. Nature Protocols. 2017 Feb;12(2):255–278. PMID: 28079879. Available from: https://doi.org/10.1038/nprot.2016.169.
33. Laskowski RA. Protein structure databases. Molecular Biotechnology. 2011 Jun;48(2):183–198. PMID: 21225378. Available from: https://doi.org/10.1007/s12033-010-9372-4.
34. Vangone A, Bonvin AM. Contacts-based prediction of binding affinity in protein-protein complexes. eLife. 2015 Jul;4:e07454. PMID: 26193119. Available from: https://doi.org/10.7554/eLife.07454.
35. Bowers KJ, Chow E, Xu H, Dror RO, Eastwood MP, Gregersen BA, et al. Scalable algorithms for molecular dynamics simulations on commodity clusters. In: Proceedings of the 2006 ACM/IEEE Conference on Supercomputing (SC '06). Tampa, FL: IEEE; 2006. p. 84. Available from: https://doi.org/10.1145/1188455.1188544.
36. Johnston RC, Yao K, Kaplan Z, Chelliah M, Leswing K, Seekins S, et al. Epik: pKa and protonation state prediction through machine learning. Journal of Chemical Theory and Computation. 2023 Apr;19(8):2380–2388. PMID: 37023332. Available from: https://doi.org/10.1021/acs.jctc.3c00044.
37. Shuaib H, Saleem Z, Alshahrani M, Suliman M, Hani U, Khan T, et al. Development and Bioactivity Assessment of a Recombinant Pseudomonas aeruginosa Azurin-BR2 Peptide Fusion Protein: A Novel Approach to Cancer Immunotherapy. Journal of Biological Regulators and Homeostatic Agents. 2024;38:5573–5581.
38. Sakurai Y, Mizuno T, Hiroaki H, Gohda K, Oku J, Tanaka T. High thermal stability imparted by a designed tandem Arg-Trp stretch in an alpha-helical coiled coil. Angewandte Chemie International Edition. 2005 Sep;44(38):6180–6183. PMID: 16124025. Available from: https://doi.org/10.1002/anie.200500806.
39. Zahreddine H, Borden KL. Mechanisms and insights into drug resistance in cancer. Frontiers in Pharmacology. 2013 Mar;4:28. PMID: 23504227. Available from: https://doi.org/10.3389/fphar.2013.00028.
40. Chabner BA, Roberts TG. Timeline: chemotherapy and the war on cancer. Nature Reviews Cancer. 2005 Jan;5(1):65–72. PMID: 15630416. Available from: https://doi.org/10.1038/nrc1529.
41. Chen J, Sawyer N, Regan L. Protein-protein interactions: general trends in the relationship between binding affinity and interfacial buried surface area. Protein Science. 2013 Apr;22(4):510–515. PMID: 23389845. Available from: https://doi.org/10.1002/pro.2230.
42. Agius R, Torchala M, Moal IH, Fernández-Recio J, Bates PA. Characterizing changes in the rate of protein-protein dissociation upon interface mutation using hotspot energy and organization. PLOS Computational Biology. 2013;9(9):e1003216. PMID: 24039569. Available from: https://doi.org/10.1371/journal.pcbi.1003216.
43. Lubkowski J, Sonmez C, Smirnov SV, Anishkin A, Kotenko SV, Wlodawer A. Crystal structure of the labile complex of IL-24 with the extracellular domains of IL-22R1 and IL-20R2. Journal of Immunology. 2018 Oct;201(7):2082–2093. PMID: 30111632. Available from: https://doi.org/10.4049/jimmunol.1800726.
44. Laskowski RA, Jabłońska J, Pravda L, Vařeková RS, Thornton JM. PDBsum: structural summaries of PDB entries. Protein Science. 2018 Jan;27(1):129–134. PMID: 28875543. Available from: https://doi.org/10.1002/pro.3289.
45. Jones S, Thornton JM. Analysis of protein-protein interaction sites using surface patches. Journal of Molecular Biology. 1997 Sep;272(1):121–132. PMID: 9299342. Available from: https://

doi.org/10.1006/jmbi.1997.1234.

46. Sørensen HP, Mortensen KK. Advanced genetic strategies for recombinant protein expression in Escherichia coli. Journal of Biotechnology. 2005 Jan;115(2):113–128. PMID: 15607230. Available from: https://doi.org/10.1016/j.jbiotec.2004.08.004.
47. Sørensen HP, Mortensen KK. Soluble expression of recombinant proteins in the cytoplasm of Escherichia coli. Microbial Cell Factories. 2005 Jan;4(1):1. PMID: 15629064. Available from: https://doi.org/10.1186/1475-2859-4-1.
48. Dutta S, Bose K. Protein purification by affinity chromatography. Textbook on Cloning, Expression and Purification of Recombinant Proteins. Singapore: Springer; 2022. Available from: https://doi.org/10.1007/978-981-16-4987-5_6.
49. Correia MT, Paiva PM, Coelho LC, Santos AF, Napoleão TH. Protein Purification. InTech; 2012.
50. Schwarz E, Beigel F. HCC tumor growth is inhibited by IL-29 in an orthotope murine tumor model: FV219. Onkologie. 2010;33(Suppl 2):147.